Revue des Composites et des Matériaux Avancés-Journal of Composite and Advanced Materials
Vol. 36, No. 1, February, 2026, pp. 209-218
Journal homepage: http://iieta.org/journals/rcma

Electrospun Nanofibres of Alginate, Polyvinyl Alcohol, and Nanohydroxyapatite as a Coating of Titanium Implant to Enhance Osseointegration

Ishraq A. Kadhim[1], Zinah A. Salman[2], Osamah A. Khadhair[3], Mayyadah S. Abed[4*], Zuhair J. Abd Alameer[5]

[1] Department of Biomaterials and Prosthesis Engineering, College of Materials Engineering, University of Technology-Iraq, Baghdad 10066, Iraq
[2] Department of Fuel and Energy Technology Engineering, Technical Engineering College, Middle Technical University, Baghdad 10098, Iraq
[3] Department of Biomedical Engineering, College of Engineering, University of Warith Alanbiyaa, Karbala 56001, Iraq
[4] Department of General Materials Engineering, College of Materials Engineering, University of Technology-Iraq, Baghdad 10066, Iraq
[5] Department of Prosthetics and Orthotics Engineering, College of Engineering, University of Kerbala, Kerbala 56001, Iraq

Corresponding Author Email: Mayyadah.S.Abed@uotechnology.edu.iq

https://doi.org/10.18280/rcma.360120

Received: 25 July 2025
Revised: 25 September 2025
Accepted: 16 February 2026
Available online: 28 February 2026

Keywords:
sodium alginate, nanohydroxyapatite, electrospinning, nanofibers, osseointegration, polyvinyl alcohol

ABSTRACT

Despite significant advancements in orthopedic implant technology, the achievement of optimal early osseointegration in titanium implants remains a challenge. This study aims to investigate the potential of a surface coating in accelerating in vitro osteogenesis on titanium implants, which were initially coated with sodium alginate (SA) and a polyvinyl alcohol (PVA) solution supplemented with nano-Hydroxyapatite (nHA). The effectiveness of each coating solution was assessed through various analyses: Fourier Transform Infrared Spectroscopy (FTIR), field emission scanning electron microscope (FESEM), Medical Training Therapy (MTT), Atomic Force Microscope (AFM), and contact angle measurements. By modifying the coating on the titanium implant, it was possible to create a hydrophilic and nanostructured surface that has the potential to enhance cell viability. The results demonstrate that SA/PVA/nHA synthesized via the electrospinning process, in combination with titanium implants, shows promise as a suitable candidate for orthopedic implants with improved osseointegration.

1. INTRODUCTION

Implantable biomaterials are frequently used to replace damaged joint tissues, reduce pain, and restore function. Examples of these implants are hip and knee replacement implants. Throughout the past few decades, totally predictable implant longevity has resulted in favourable clinical outcomes; yet, more than half of implant failures have been attributable to prosthesis displacement inside the host bone [1].

Cobalt chromium alloys, stainless steel, and titanium alloys are the most potent varieties of implantable metallic biomaterials. Titanium and its alloys are among those materials that have the most interest due to their remarkable mechanical properties, exceptional resistance to corrosion, excellent strength, and relatively low weight. They also have the best biocompatibility of any alloy [2].

Orthopaedic implants are preferable to bone transplants in cases of flaws and bone injuries since they may provide mechanical stability for the building structure of bone, aiding in pain relief and functional rehabilitation [3]. Nonetheless, it is critical to enable rapid peri-implant healing in several clinical applications. It is thought that improving the surface characteristics of implants can encourage early osseointegration by facilitating the attachment of bone-forming cells [4].

Modifying the surface is the simplest way to improve the biological qualities since it increases the bioactivity surface, prevents infections brought on by implants, and eliminates or controls the pace of degradation, while the desired properties of the materials are preserved [5].

One excellent option for scaffolding that has positive biological features is electrospun scaffolds. The permeability, scar formation control, and extracellular matrix (ECM)-like structure of electrospun nanofibres are extraordinary features [6].

Alginates are abundant in sources, non-toxic, and accessible, with their biocompatibility and biodegradability in the human body having been demonstrated. They have been widely employed in the food sector and have developed into crucial biomaterials for pharmacological and biological purposes due to these advantageous qualities [7]. Owing to these beneficial characteristics, alginates have been extensively used in the food industry and have become essential biomaterials for pharmacological and biological purposes. Because of their high biocompatibility and biological origin, alginates are frequently used in the tissue

engineering field, especially in the repair of bone, skin, cartilage, and wounds [8].

PVA is a synthetic, water-soluble biopolymer, with excellent mechanical and thermal characteristics, clarity, and oxygen resistance [9]. The field of medical coating technology has recently become quite interested in bioactive calcium phosphate due to its crucial function in enhancing the interaction between the implant and the surrounding tissue [10]. PVA-based electrospun nanofibrous scaffolds have been widely studied for tissue engineering applications [11].

The precipitation of hydroxyapatite nanoparticles into metallic implants enhanced the applications for orthopaedics by producing bio-materials with physiochemical properties and high levels of bioactivity and biocompatibility on the surface [12]. The incorporation of nano-Hydroxyapatite (nHA) in the scaffold enhances its bioactivity and promotes bone regeneration [13]. The effect of nHA concentration and size on the morpho-mechanical properties of an electrospun scaffold has also been studied, where it was found that increasing the nHA concentration resulted in an increase in fibre diameter and a decrease in pore size. However, increasing the nHA size had no significant effect on fibre diameter or pore size [14].

In a different study, it was found that Coaxial electrospun polycaprolactone (PCL)/polyvinyl alcohol (PVA) core-sheath nanofibre (NF) with both collagen (Col) and hydroxyapatite nanorods (HA), adhered strongly to the titanium rod surface and that the nanofibre coating remained intact after implantation using an ex vivo porcine bone implantation model [15]. Another study involved creating chitosan/zein composite films with ellagic acid to treat skin infections and speed up skin recovery. The formed films had a high rate of water uptake, making them appropriate for dressing wounds [13].

Electrospun nanofibres of alginate, PVA, and nanohydroxyapatite have been studied in this work as a coating for titanium scaffolds to enhance osseointegration. While there is limited research that specifically addresses this combination of materials, there are related studies on electrospun nanofibres made from PVA and HA, which have been shown to improve osseointegration in bone implantation models. To promote osseointegration of coated implants with bone via cell culture, this work aimed at obtaining a titanium implant coated with sodium alginate (SA), PVA, and reinforced with bioactive ceramic nanohydroxyapatite (MCF-7).

2. EXPERIMENTAL PART

2.1 Materials

The SA powder, which is alginic acid sodium salt derived from brown algae, with a medium molecular weight and medium viscosity (Formula: $(C_6H_8O_6)n$, was obtained from Sigma-Aldrich/USA. PVA, with a high molecular weight, high viscosity, and water solubility (Formula: $[-CH_2CH(OH)-]n$, was supplied by Alfa Aesar-Thermo Fisher Scientific/USA. The nano hydroxyapatite powder, consisting of particles with a size of 20nm and a needle-like shape, with a purity of 97.5%, was purchased from Shanghai Theorem Chemical Technology Co., Ltd., located in Shanghai, China. The raw material for the screw used in the study was pure titanium (99.8%).

2.2 Preparation of titanium screw

A pure titanium rod was used as the substrate, and the implant screw was fabricated by machining the titanium rod, as illustrated in Figure 1. The surface of the screw was chemically treated by immersion in a concentrated acidic solution to increase the roughness of the surface of the titanium screw and enhance its bioactivity within the human body. The samples were etched in 48% H_2SO_4 at 60°C for one hour, washed in water, ultrasonically cleaned with acetone, 70% ethanol, and distilled water, dried in air at room temperature, and kept sterile to prevent contamination. This process removes surface contamination and exposes the underlying material [16, 17].

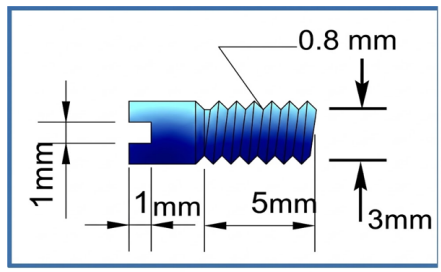

Figure 1. Screw implant design

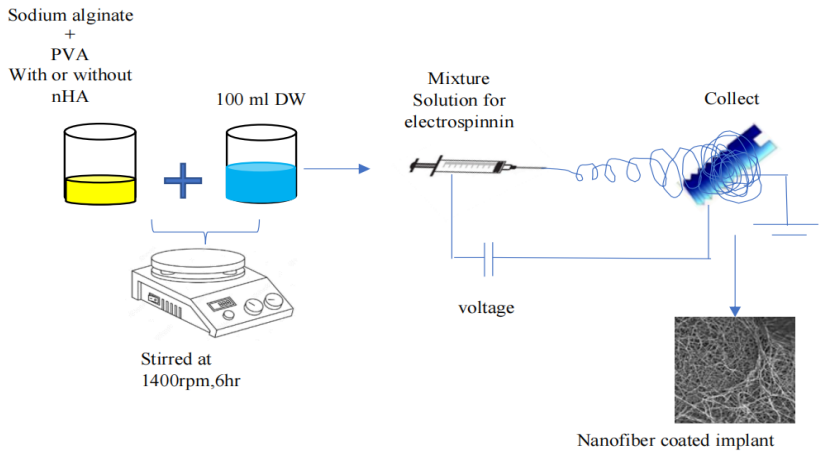

Figure 2. Schematic diagram of the current coating process
Note: produced by the authors themselves

Table 1. Composition of electrospinning solutions

Sample Code	Screw Base	SA/PVA	nHA
A	Ti	-	-
B	Ti	3:1	-
C	Ti	3:1	0.1 g
D	Ti	3:1	0.2 g
E	Ti	3:1	0.3 g

Note: sodium alginate (SA); polyvinyl alcohol (PVA); nano-Hydroxyapatite (nHA)

2.3 Preparation of electrospun nanofibre (coating)

Both SA and PVA were diluted in 100 mL of distilled water in the amounts required to produce electrospinning solution concentrations of (2.5% w/v) as well as (5% w/v), respectively. For 6 hours, the solution was stirred at 1400 rpm using a magnetic stirrer. Powdered nHA was added to the mixture. Finally, 5 mL of the solution was poured into a syringe to make sure it was thoroughly mixed and bubble-free. Flow rate (1 mL/h), voltage (25 kV), and needle-holder distance (15 cm) were the conditions used for electrospinning. To guarantee that every rod received an electrospinning coat, the titanium was mounted in a holder. Bio-electrospinning equipment was used to carry out the electrospinning procedure [18-21]. Figure 2 is a schematic diagram of the current coating process.

Table 1 illustrates the composition of the prepared samples. Figure 3 shows the coated and uncoated Ti implants.

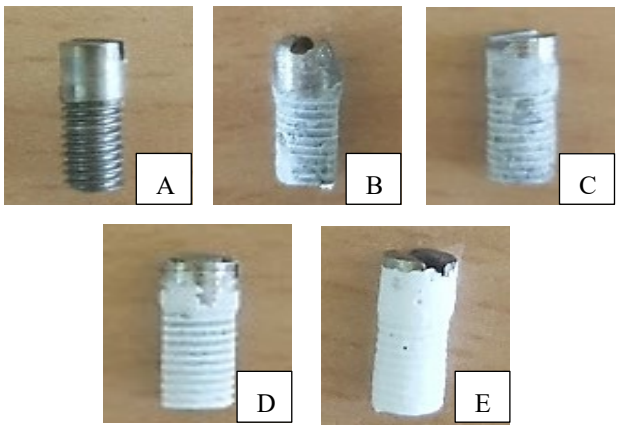

Figure 3. Titanium implants, A) sample A (uncoated), B-E) coated samples; B, C, D, and E

2.4 Laboratory testing and characterisation

2.4.1 Morphology assay

Field emission scanning electron microscope (FESEM) equipment, model Inspect F50/FEI company, USA, was used to characterise the surface of a titanium screw coated with electrospinning film. Inspection conditions were 5 kV acceleration voltage and 35–70 kX as magnification. The average diameter was calculated via Image J software.

2.4.2 Atomic Force Microscope

The surface topography of the coated nanofibre on the titanium implant was characterised using the tapping mode of Atomic Force Microscope (AFM) (NaioAFM 2022, Nanosurf, Switzerland). In the non-contact mode, SPM images of the sample surface were taken from a distance of (0.1–10 nm). The arithmetic average of the values in the roughness profile was used to estimate roughness (Ra). WSxM 4.0 software was used to assess the AFM analysis.

2.4.3 Miscibility assay

An infrared spectrometer, Transform Infrared Spectroscopy (FTIR) was used to check each coating's bonding of the SA and PVA components. The test was carried out using an apparatus made by the Bruker Optics Corporation (Germany), type Tensor-27. The Titanium screw that was not coated was used as a reference. The specimen was put into the apparatus, and the test was run in the air at a normal temperature. This apparatus uses a KBr beam splitter and a mid-IR source with a wavelength of 4000 cm^{-1}–400 cm^{-1}.

2.4.4 Hydrophilicity assay

The contact angle was calculated to figure out and compare the coating's wettability. Using a contact angle measuring device (Crating Nano Technologies Inc., Model CAM120, Taiwan) and deionised water dropped onto the coated surface at 25°C, the wettability of the samples was evaluated. A monitoring program has been used in further testing on the digital screen to assess the contact angle.

2.4.5 Cell viability assay

In brief, the human cell MCF-7 were injected at 104 cells per 96-well tissue culture plate and maintained for 24 hours in 100 l of DMEM/F12, which was achieved with 10% Fetal bovine serum FBS. After that, the MCF-7 cells were grown for 24 hours in a brand-new serum culture media that included dilutions of the implants over time. The cells were then cultured for an additional 24 hours in the full medium before the media were replaced with 00 l of implants and 100 l of medium containing 0.5 mg/mL Medical Training Therapy (MTT) solution. After 24 hours, the medium was removed, 100 l of DMSO was used to dissolve live cell-produced MTT formazan, and the absorbance 570 nm was measured using a microplate reader. The absorbance values from the control wells and the implant-treated wells were used to compute the cell viability % ([A] test and [A] control, respectively). The data are shown as the mean SD (n = 3) [22].

3. RESULTS AND DISCUSSION

3.1 Morphology observation

The surface morphology was investigated for coated and uncoated samples using FESEM images at a magnification of 3 kX (see Figure 4). The uncoated screw implant displayed a smooth surface (Figure 4A), while the coated surfaces exhibited a rough texture (Figures 4(B, C, D, and E)). It was evident that all the coated samples possessed a complete coverage of nanofibres on their surfaces. Particularly, the SA/PVA coating displayed smooth, elongated fibres without any discontinuities or nodes (Figure 4B). The SA/PVA scaffolds demonstrated a porous structure with interconnected pores and uniform nanofibres that were randomly oriented, exhibiting an average diameter of 256.7 nm. Conversely, when nano nHA was incorporated, a distinct tangled network with nodes was observed (Figures 4(C, D, and E)). The addition of nHA resulted in a uniform distribution of nHA on the nanofibre surfaces without blocking the pores on the scaffold's surface [14, 23-26].

FESEM images of the coated titanium screws (see Figure 5) were captured at two different magnifications (35 and 70 kX). The results shown in this figure are consistent with those shown in the preceding figure. The SA/PVA electrospun nanofibrous mats have no bead formations and a continuous, nonwoven structure with interconnected porous morphology. The neat SA/PVA blend gives more uniform nanofibers, a smooth and homogeneous surface, with an average diameter of 150 ± 50 nm, as in Figure 5(B1 and B2). It is related that the functional groups of alginates form hydrogen bonds with PVA, resulting in a more stable and defect-free nanofibre morphology [27].

Whereas it was noticed the aggregated mass within fibers was observed when incorporating nHA particles within the polymer blend matrix. As illustrated in (Figure 5(C2, D2, E2)), the inclusion of HA nanoparticles leads to a reduction in the average diameter of the nanofibres to 100 ± 50 nm, 85 ± 50 nm, and 70 ± 40 nm for composite nanofibres (SA/PVA/0.1 nHA, SA/PVA/0.2 nHA, SA/PVA/0.3 nHA), respectively. The surface of these fibres appears rougher compared to the neat polymer blend fibres (SA/PVA) due to the presence of HA nanoparticles. This nanofibres' roughness is expected to enhance surface wettability, facilitate bone cell barrier, and promote osteogenic differentiation [25].

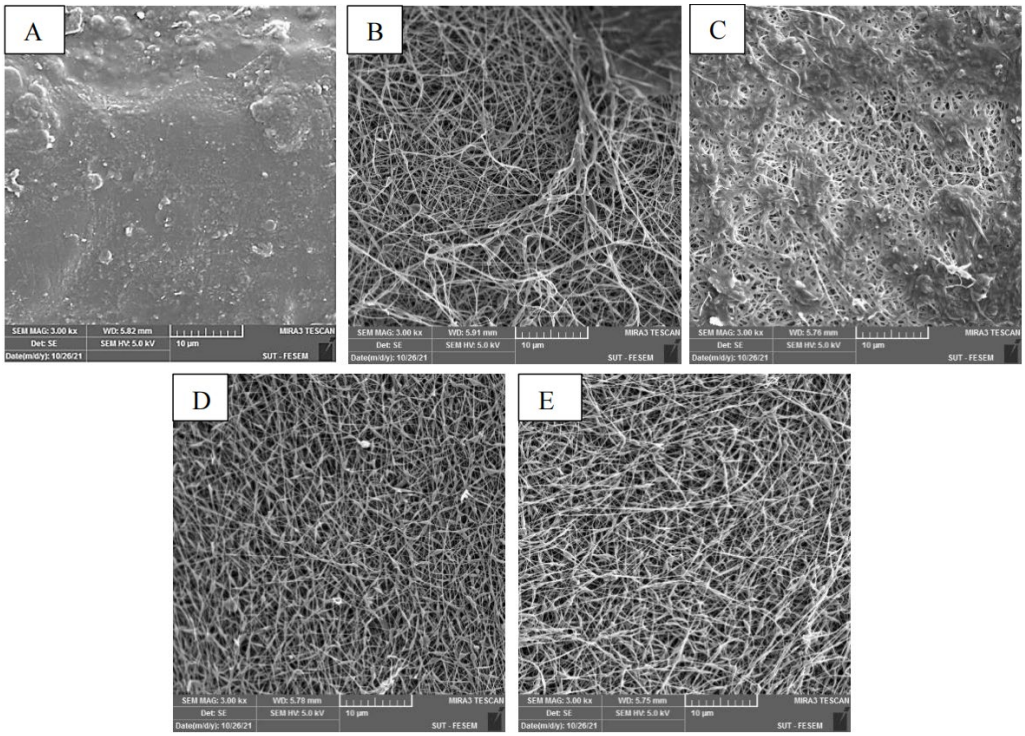

Figure 4. Field emission scanning electron microscope (FESEM) images of the (A) uncoated sample, and (B, C, D and E) coated samples at magnifications (3 kX)

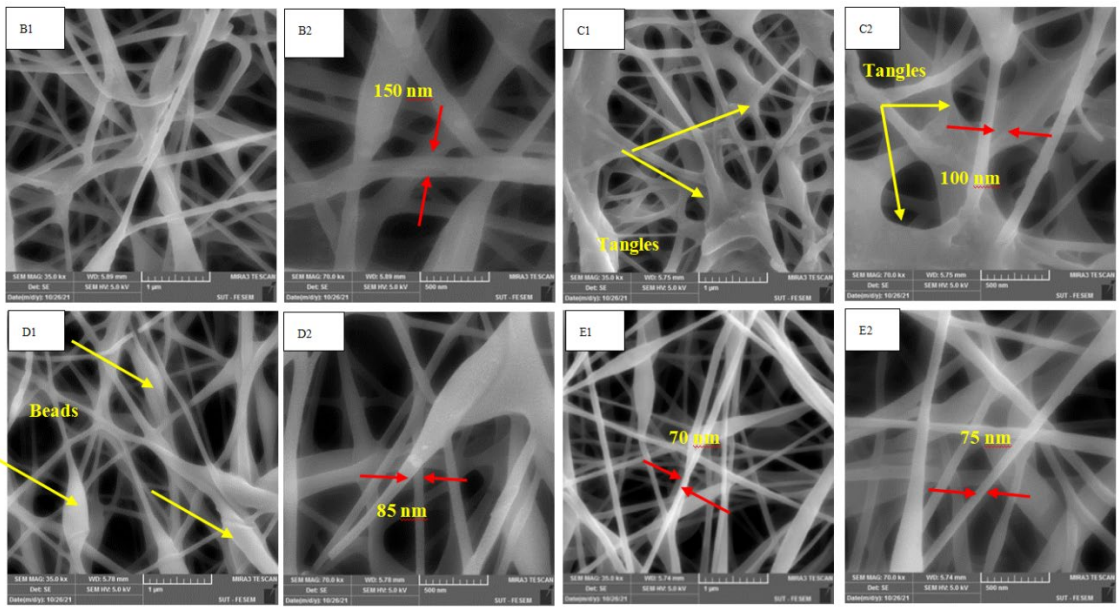

Figure 5. Field emission scanning electron microscope (FESEM) images of the coated samples (B, C, D, and E) at different magnifications (35 and 70 kX); sample B: Thicker and less tangled fibres with no beads, sample C: Shorter and highest tangled fibres, sample D: More uniform and continuous fibres with less tangles and beads

Also, cylindrical fibres with reduced tangles were observed for fibres electrospun from the SA/PVA blend (sample B). Whereas, in the case of fibres electrospun from the SA/PVA/nHA mixture, finer and shorter fibres were observed, indicating an increase in fibre fineness (sample C). Further increasing the nHA content led to finer and more uniform fibres, accompanied by the presence of spindle-shaped and round beads (sample D). An additional increase in nHA content resulted in the electrospinning of more uniform, finer, and continuous fibres, with reduced tangles and significantly fewer beads (sample E). These SEM observations provide evidence of improved fiber uniformity and a decreased presence of bead structures with increasing nHA content, demonstrating favorable electrospinning efficiency [27].

The thicker fibres observed in SA/PVA blends suggest the occurrence of intermolecular interactions between SA and PVA, likely through hydrogen bonding among the numerous hydroxyl and carboxyl groups of SA and PVA hydroxyl groups. The fibre-forming ability of these mixtures indicates that PVA chains not only entangle with each other but also interact with SA or enhance SA-PVA chain entanglement. The addition of hydroxyapatite to the blends increases hydrogen bonding and intermolecular attraction between HA-PVA and HA-SA, leading to a more entangled electrospinning process (sample C). However, with further increases in nHA content, a balance is achieved between fibre repulsion and attraction, resulting in the facile electrospinning of more uniform and finer fibres.

The formation of certain noticeable agglomerates is attributed to the high surface energy of the nano-sized HA particles [28]. The successful modification and adhesion between the substrate and coating are evidenced by the complete coverage of the screw implant surface through electrospinning. Table 2 provides details of the fibre diameter and pore size, which were determined using the Image J program. The surface of the screw implant exhibits a range of membrane nanofibre diameters and pore sizes, with values ranging from 100 nm to 250 nm for diameter ($100 \leq D \leq 250$ nm) and from 120 nm to 225 nm for pore size ($120 \leq P \leq 225$ nm).

Table 2. Fibre diameters and pore size of the scaffolds

Sample Code	Fibre Diameter (nm)	Pore Size (nm)
B	156.7	224.7
C	111.5	190.8
D	97.8	135.3
E	75.4	123.7

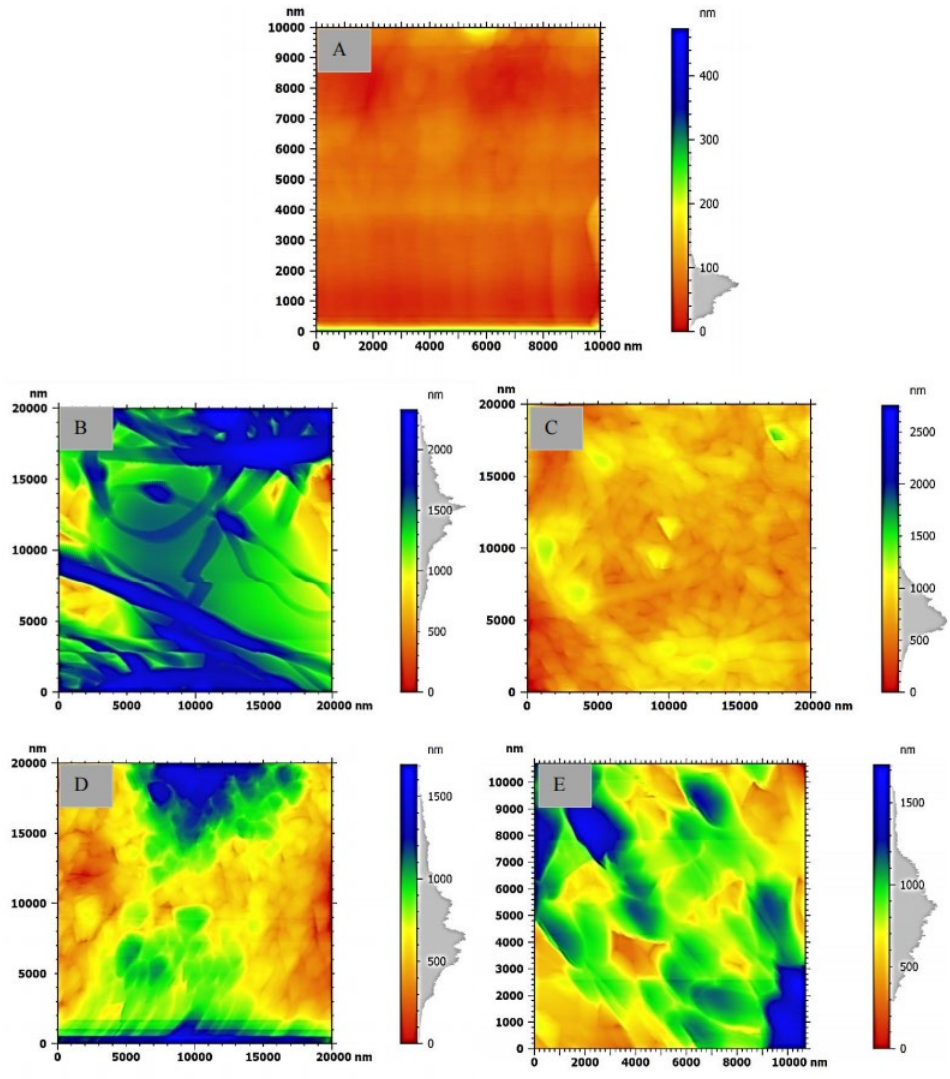

Figure 6. Pseudo colored 2D topography image by Atomic Force Microscope (AFM) analysis of uncoated and coated titanium implants (samples A, B, C, D, and E)

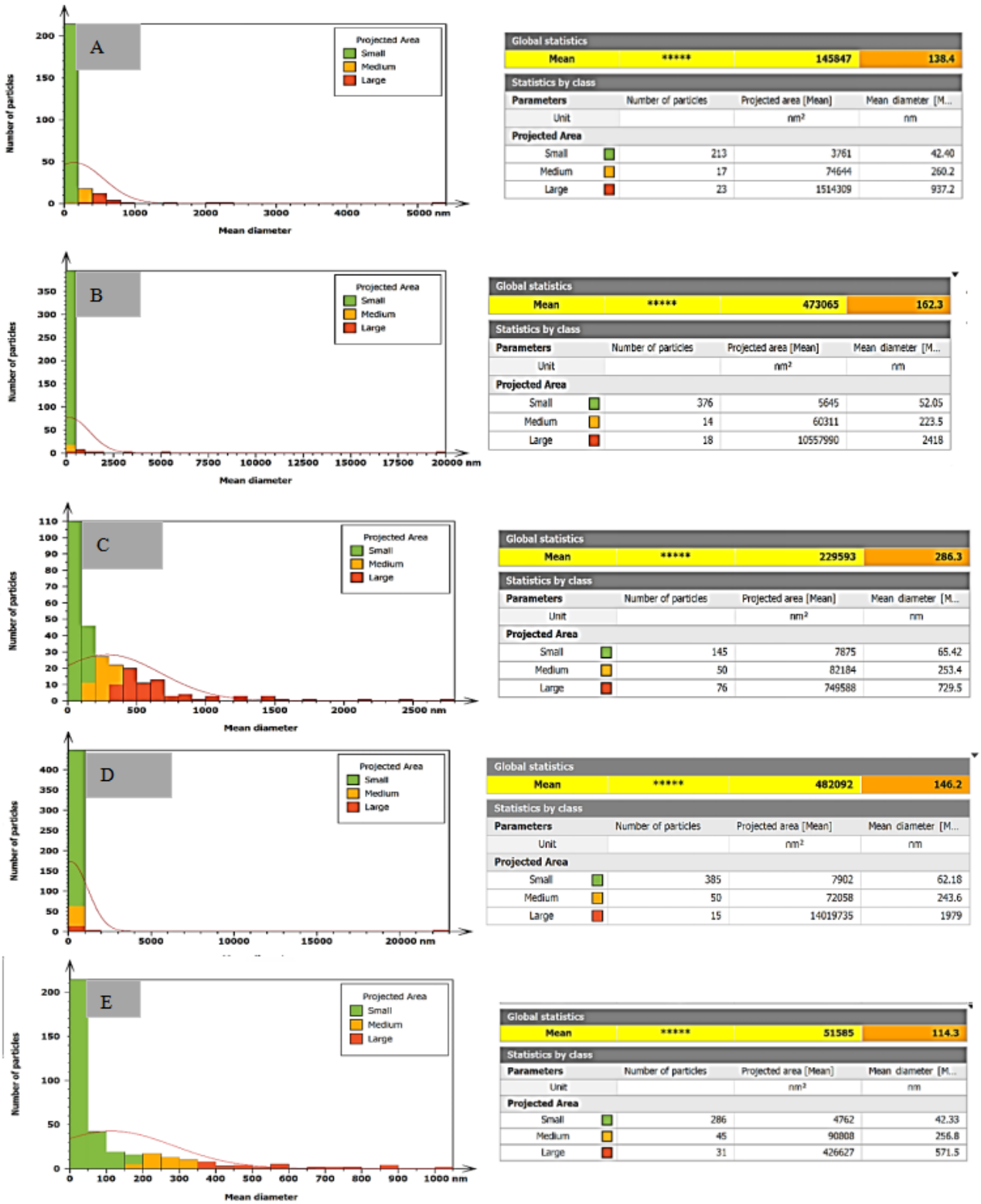

Figure 7. Atomic Force Microscope (AFM) of titanium implant and coated

3.2 Atomic Force Microscope analysis

AFM results involve the surface roughness and particle size analyses with related pseudo 2D topography images.

3.2.1 Surface roughness

Figure 6 depicts the 2D images of the uncoated and coated titanium implants (samples A, B, C, D, and E), while Table 3 presents the height parameters used as indicators for surface roughness assessment. The main parameters considered are root mean square height (Sq), maximum height (Sz), and arithmetic mean height (Sa). The uncoated implant (sample A) exhibits a smooth surface, as clearly observed. However, after coating the surface with the long fibres of the SA/PVA blend (Figure 6B), the roughness increases by approximately 1100%, consistent with the related SEM observation. The utilization of SA/PVA solution leads to the production of more uniform fibres without beads and thick fibrous mats [27].

Surface roughness of the coated sample increases by approximately 600% when nHA was incorporated within

polymer blends compared to the uncoated sample (sample C). Although the surface roughness of Pure SA/PVA (sample B) is higher than that of SA/PVA/nHA (sample C). It may be attributed to the average diameter reduction of the nanofibres resulting from the inclusion of HA nanoparticles.

Table 3. Atomic Force Microscope (AFM) height parameters of electrospun titanium implants

Sample	Sq Root Mean Square Hight (nm)	Sz Maximum Hight (nm)	Sa Arithmetic Mean Height (nm)
A	31.47	473.2	21.09
B	336	2330	260.7
C	204.7	2753	150.2
D	281.8	1694	224.0
E	258.2	1731	203.2

Additionally, the increased intermolecular hydrogen bonding among HA-PVA and HA-SA (as discussed in the SEM observations) leads to enhanced fibre entanglement and improved material continuity on the surface, thereby reducing the surface roughness.

Further addition of nHA (0.2 g nHA for sample D, and 0.3 g nHA for sample E) makes electrostatic balance among fibres, resulting in finer fibres with reduced tangles and increased surface roughness compared to sample C (0.1 g nHA). Consequently, the surface roughness increases by only approximately 967% and 867% for samples D and E, respectively, when compared to the uncoated sample (sample A).

3.2.2 Particle size analysis

Figure 7 presents the histogram of particle size analysis along with the corresponding legend table for all samples (A, B, C, D, and E). It is important to note that in the context of coated surfaces, the term "particle" refers to the fibre diameter itself, as there are no actual particles present.

For the uncoated sample (sample A), at a projected area of 3761 nm, there are 213 small particles with a mean diameter of 42.40 nm. At a projected area of 74644 nm, there are only 17 medium-sized particles with a mean diameter of 260.2 nm, and at a projected area of 1514309 nm, there are only 23 large-sized particles with a mean diameter of 937.2 nm. This indicates that 84% of the surface particles are of similar size, and the mean diameter across all projected areas is approximately 138.4 nm.

Sample B comprises particles with a mean diameter of 53.05 nm, where approximately 92% of the particles fall into the small size category, while 8% belong to the medium and large size categories. The mean diameter for all projected areas is determined to be 162.3 nm. In the case of sample C, the mean diameter is 286.3 nm, with around 53% of the particles falling within the small size range and approximately 47% categorized as medium and large-sized. As for sample D, it has a mean diameter of 146.2 nm, with approximately 85% of the particles being small-sized and 15% being medium and large-sized.

Lastly, for sample E, approximately 77% of the particles are within the small size range (mean diameter of 42.33 nm), while about 33% refer to medium and large-sized particles, resulting in a mean diameter of 114.3 nm for all projected areas. Table 4 summarizes the mean particle sizes for the coated and uncoated samples.

Table 4. Atomic Force Microscope (AFM) particle size analysis summary

Sample	Mean Diameter
A	138.4
B	162.3
C	286.3
D	146.2
E	114.3

It is evident that the mean diameter increases when the implant is coated with fibres via electrospinning. This size specifically refers to the fibre diameter. Sample C exhibits a higher mean diameter due to the AFM tip sensing both the fibre diameter and tangled regions, which increases the calculated size. Sample E demonstrates the smallest mean diameter, indicating the generation of finer fibres. These observations align with the SEM observations and are consistent with the provided explanations.

3.3 Fourier Transform Infrared Spectroscopy analysis

Figure 8 shows the FTIR spectra of all the coated implants. The uncoated implant (sample A) is chosen as the control sample, because the remaining samples were coated with the same ratio of SA/PVA. Peaks at similar regions are visible in the electrospun SA /PVA. Between 1500 and 3600 cm^{-1} wavelengths are the defining bands for alginate. The stretching band of hydroxyl group O-H and the stretching of the C-H band are responsible for the peaks that appear at 3291 and 2913 cm^{-1}, respectively, whilst the C≡N group is responsible for that at 1088 cm^{-1}. The carboxylate group is responsible for the significant peak at 1717 cm^{-1}. A variation between peak intensity in the SA /PVA coating is seen at 1135 cm^{-1}. The peaks 820, 901, 1316, 1418, 1629, 2962, and 3445 $cm^{-1}$are in the C-C stretching band. These wavelengths appear in SA/PVA/nHA samples. Due to the presence of a polymer base (Alginate), the peak broadening of PO_4 is visible around 900 - 1200 cm^{-1} [29]. Bending OH-groups appear at about 969–965 cm^{-1}. While the peaks from 1700-1550 cm^{-1}correspond to the stretching of the carboxylic group COO- [30].

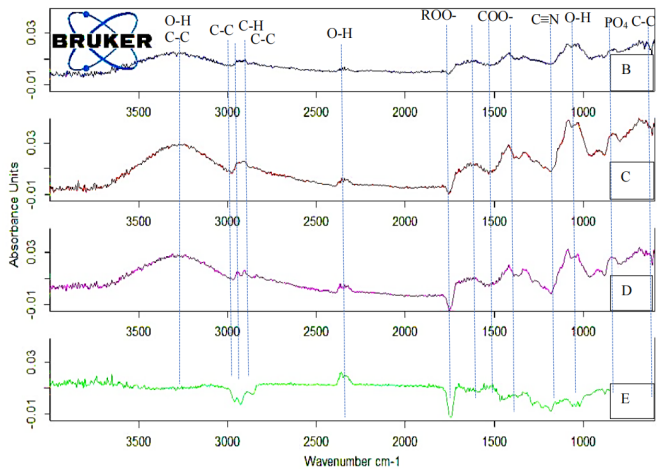

Figure 8. Fourier Transform Infrared Spectroscopy (FTIR) analysis of the coated samples B, C, D, and E

3.4 Hydrophilicity assay

Establishing osseointegration, which involves achieving a strong bond between the implant surface and the surrounding

bone, is a critical clinical objective in orthopedics for assessing the effectiveness of bone implants. Various surface modification techniques have been developed to enhance osseointegration. However, considering implant wettability as an important biological characteristic, it remains poorly understood due to insufficient findings by researchers [31]. The findings from the contact angle analysis are presented in Figure 9. The contact angle was measured at 25° for the SA/PVA-coated titanium screw (sample B), indicating a higher hydrophilicity. The contact angles increased to 30°, 32°, and 35° with the incorporation of nHA into the SA/PVA-coated screw (samples C, D, and E), respectively. This is attributed to the hydrophilic nature of hydroxyapatite, which contributed to maintaining the hydrophilic character of the coating rather than changing it.

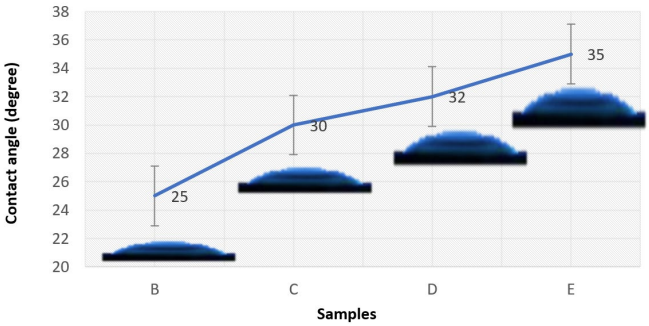

Figure 9. Contact angle for the coated samples

The reported contact angles for the coated membranes are below 50°, indicating their exceptional hydrophilicity resulting from the hydrophilic properties of SA, PVA, and nHA. The low contact angles observed in all samples indicate their high hydrophilicity, making them highly suitable for cell adhesion. Consequently, gaining a better understanding of the wetting mechanisms of implant surfaces is increasingly important.

3.5 Cell viability assay

It is necessary to evaluate the biocompatibility and cytotoxicity of any tissue engineering implants. In this study, the cell viability assay for SA/PVA/nHA electrospun-coated titanium implants was investigated to ensure osseointegration. The viability of the MCF-7 cell line was examined using the MTT assay at 24, 48, and 72 hours, as depicted in Figure 10. The graph presents the MTT results for a coated implant. In comparison to the uncoated sample A, which consistently exhibited high levels of cell viability across all time points.

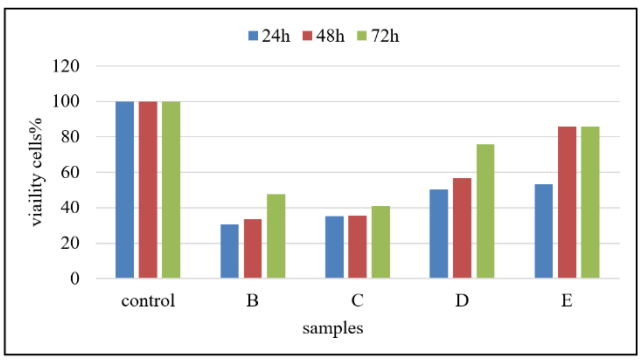

Figure 10. Cell viability of implants

Excellent biocompatibility was shown by samples B, C, D, and E when cell viability over time increased. The findings suggest that all screw implants, including the scaffolds, have the potential to promote osseointegration and are suitable for orthopedic implant applications. Notably, there were no discernible differences in cell viability between the coated samples and the control group in the MTT experiment. Additionally, it can be concluded that all implants showed favorable cell adherence based on assessments of cell development and cell concentration [32, 33].

4. CONCLUSIONS

In conclusion, the use of surface coatings shows promise in improving the performance of orthopedic implants and reducing the risk of complications. Despite substantial developments in orthopedic implant technology, designing titanium implants with the best early osseointegration remains a challenge. The electrospinning process has been used to successfully create stable coating precipitation on titanium rods, and the SA/PVA/nHA synthesized using the electrospinning process, and titanium implants are satisfactory candidates for orthopedic implants with enhanced osseointegration. The findings show that by modifying the coating on the titanium implant, a hydrophilic and nanostructured surface can be produced, which could promote cell viability. The fibrillar structure has the potential to increase the biocompatibility of titanium implants. Analysis of the morphology and coating stability has revealed remarkably stable coatings. The results from in vitro assays have demonstrated that cells seeded on coated implants display higher cell adhesion, proliferation, and surface cytocompatibility. This concept could prove highly effective when applied to the fields of antibacterial dentistry and orthopaedics.

ACKNOWLEDGEMENTS

The authors would like to thank and appreciate all the valuable efforts of all colleagues in the College of Materials Engineering, University of Technology-Iraq, who have provided a benefit and helpful support, which led to the achievement and improvement of this work.

REFERENCES

[1] Sukhodub, L., Sukhodub, L.B., Kumeda, M., Panda, A., Baron, P. (2020). ZnO coatings on Ti6Al4V substrate: Structural and antibacterial properties in literature review and research. Management Systems in Production Engineering, 28(4): 318-324. https://doi.org/10.2478/mspe-2020-0045

[2] Qin, L., Liu, C., Yang, K., Tang, B. (2013). Characteristics and wear performance of borided Ti6Al4V alloy prepared by double glow plasma surface alloying. Surface and Coatings Technology, 225: 92-96. https://doi.org/10.1016/j.surfcoat.2013.02.053

[3] Raphel, J., Holodniy, M., Goodman, S.B., Heilshorn, S.C. (2016). Multifunctional coatings to simultaneously promote osseointegration and prevent infection of orthopaedic implants. Biomaterials, 84: 301-314.

https://doi.org/10.1016/j.biomaterials.2016.01.016
[4] Jia, L., Han, F., Wang, H., Zhu, C., et al. (2019). Polydopamine-assisted surface modification for orthopaedic implants. Journal of Orthopaedic Translation, 17: 82-95. https://doi.org/10.1016/j.jot.2019.04.001
[5] Su, Y., Wang, K., Gao, J., Yang, Y., Qin, Y.X., Zheng, Y., Zhu, D. (2019). Enhanced cytocompatibility and antibacterial property of zinc phosphate coating on biodegradable zinc materials. Acta Biomaterialia, 98: 174-185. https://doi.org/10.1016/j.actbio.2019.03.055
[6] Keirouz, A., Chung, M., Kwon, J., Fortunato, G., Radacsi, N. (2020). 2D and 3D electrospinning technologies for the fabrication of nanofibrous scaffolds for skin tissue engineering: A review. Wiley Interdisciplinary Reviews: Nanomedicine and Nanobiotechnology, 12(4): e1626. https://doi.org/10.1002/wnan.1626
[7] Hernández-González, A.C., Téllez-Jurado, L., Rodríguez-Lorenzo, L.M. (2020). Alginate hydrogels for bone tissue engineering, from injectables to bioprinting: A review. Carbohydrate Polymers, 229: 115514. https://doi.org/10.1016/j.carbpol.2019.115514
[8] Abd, I., Kadhim, U. (2021). Biocompatibility of alginate-graphene oxide film for tissue engineering applications. Key Engineering Materials, 900: 26-33.
[9] Abdullah, Z.W., Dong, Y. (2019). Biodegradable and water resistant poly (vinyl) alcohol (PVA)/starch (ST)/glycerol (GL)/halloysite nanotube (HNT) nanocomposite films for sustainable food packaging. Frontiers in Materials, 6: 58. https://doi.org/10.3389/fmats.2019.00058
[10] Jeong, J., Kim, J.H., Shim, J.H., Hwang, N.S., Heo, C.Y. (2019). Bioactive calcium phosphate materials and applications in bone regeneration. Biomaterials Research, 23(1): 4. https://doi.org/10.1186/s40824-018-0149-3
[11] Teixeira, M.A., Amorim, M.T.P., Felgueiras, H.P. (2020). Poly (vinyl alcohol)-based nanofibrous electrospun scaffolds for tissue engineering applications. Polymers, 12(7): 1-23. https://doi.org/10.3390/polym12010007
[12] Liu, D.M., Troczynski, T., Tseng, W.J. (2001). Water-based sol gel synthesis of hydroxyapatite: Process development. Biomaterials, 22(13): 1721-1730. https://doi.org/10.1016/S0142-9612(00)00332-X
[13] Eldeeb, A.E., Salah, S., Elkasabgy, N.A. (2022). Biomaterials for tissue engineering applications and current updates in the field: A comprehensive review. Aaps Pharmscitech, 23(7): 267. https://doi.org/10.1208/s12249-022-02419-1
[14] Lopresti, F., Pavia, F.C., Vitrano, I., Kersaudy-Kerhoas, M., Brucato, V., La Carrubba, V. (2020). Effect of hydroxyapatite concentration and size on morpho-mechanical properties of PLA-based randomly oriented and aligned electrospun nanofibrous mats. Journal of the Mechanical Behavior of Biomedical Materials, 101: 103449. https://doi.org/10.1016/j.jmbbm.2019.103449
[15] Song, W., Yu, X., Markel, D.C., Shi, T., Ren, W. (2013). Coaxial PCL/PVA electrospun nanofibers: Osseointegration enhancer and controlled drug release device. Biofabrication, 5(3): 035006. https://doi.org/10.1088/1758-5082/5/3/035006
[16] Jemat, A., Ghazali, M.J., Razali, M., Otsuka, Y. (2015). Surface modifications and their effects on titanium dental implants. BioMed Research International, 2015(1): 791725. https://doi.org/10.1155/2015/791725
[17] Iwaya, Y., Machigashira, M., Kanbara, K., Miyamoto, M., Noguchi, K., Izumi, Y., Ban, S. (2008). Surface properties and biocompatibility of acid-etched titanium. Dental Materials Journal, 27(3): 415-421. https://doi.org/10.4012/dmj.27.415
[18] Abd, I., Kadhim, U. (2023). Investigation of physochimechal and biological properties of composite sodium alginate for tissue engineering. Journal of Biomimetics, Biomaterials and Biomedical Engineering, 59: 11-20. https://doi.org/10.4028/p-a7ygw7
[19] Kadhm, A.A., Alameer, Z.J.A., Zubaidi, A.B.A. (2019). Enzymatic degradation of chitosan blend for tissue engineering application. AIP Conference Proceedings, 2123(1): 020017. https://doi.org/10.1063/1.5116944
[20] Kadhim, I.A., Ameer, Z.J.A., Alzubaidi, A.B. (2020). Investigation of chitosan film degradation in tissue engineering applications. IOP Conference Series: Materials Science and Engineering, 671(1): 012060. https://doi.org/10.1088/1757-899X/671/1/012060
[21] Kadhim, I.A., Zubaidi, A.B.A., Abd Alameer, Z.J., Hameed, F.M., Sadeq, A.W. (2020). Genipin cross-linked chitosan/polyvinyl alcohol blend for biomedical engineering. Indian Journal of Forensic Medicine & Toxicology, 14(3): 1656-1662. https://doi.org/10.37506/ijfmt.v14i3.10653
[22] Rençber, S., Cheaburu-Yilmaz, C.N., Aydin Köse, F., Karavana, S.Y., Yilmaz, O. (2019). Preparation and characterization of alginate and chitosan IPC based gel formulation for mucosal application. Cellulose Chemistry and Technology, 53(8): 655-665. https://doi.org/10.35812/cellulosechemtechnol.2019.53.64
[23] Song, H., Zhang, Y., Zhang, Z., Xiong, S., Ma, X., Li, Y. (2021). Hydroxyapatite/nell-1 nanoparticles electrospun fibers for osteoinduction in bone tissue engineering application. International Journal of Nanomedicine, 16: 4321-4332. https://doi.org/10.2147/IJN.S309567
[24] Seyedjafari, E., Soleimani, M., Ghaemi, N., Shabani, I. (2010). Nanohydroxyapatite-coated electrospun poly (L-lactide) Nanofibers enhance osteogenic differentiation of stem cells and induce ectopic bone formation. Biomacromolecules, 11(11): 3118-3125. https://doi.org/10.1021/bm1009238
[25] Satpathy, A., Pal, A., Sengupta, S., Das, A., et al. (2019). Bioactive nano-hydroxyapatite doped electrospun PVA-chitosan composite nanofibers for bone tissue engineering applications. Journal of the Indian Institute of Science, 99(3): 289-302. https://doi.org/10.1007/s41745-019-00118-8
[26] Sato, T.P., Rodrigues, B.V., Mello, D.C., Münchow, E.A., et al. (2021). The role of nanohydroxyapatite on the morphological, physical, and biological properties of chitosan nanofibers. Clinical Oral Investigations, 25(5): 3095-3103. https://doi.org/10.1007/s00784-020-03633-6
[27] Shen, W., Hsieh, Y.L. (2014). Biocompatible sodium alginate fibers by aqueous processing and physical crosslinking. Carbohydrate Polymers, 102: 893-900. https://doi.org/10.1016/j.carbpol.2013.10.066
[28] Wan, B., Ruan, Y., Shen, C., Xu, G., Forouzanfar, T., Lin, H., Wu, G. (2022). Biomimetically precipitated nanocrystalline hydroxyapatite. Nano TransMed, 1(2-4):

e9130008. https://doi.org/10.26599/ntm.2022.9130008
[29] Prakash, J., Kumar, T.S., Venkataprasanna, K.S., Niranjan, R., Kaushik, M., Samal, D.B., Venkatasubbu, G.D. (2019). PVA/alginate/hydroxyapatite films for controlled release of amoxicillin for the treatment of periodontal defects. Applied Surface Science, 495: 143543. https://doi.org/10.1016/j.apsusc.2019.143543
[30] Kanasan, N., Adzila, S., Suid, M.S., Gurubaran, P. (2016). Preparation and characterization of hydroxyapatite/sodium alginate biocomposites for bone implant application. AIP Conference Proceedings, 1756(1): 020006. https://doi.org/10.1063/1.4958749
[31] Strnad, G., Chirila, N., Petrovan, C., Russu, O. (2016). Contact angle measurement on medical implant titanium based biomaterials. Procedia Technology, 22: 946-953. https://doi.org/10.1016/j.protcy.2016.01.094
[32] Yadav, N., Francis, A.P., Priya, V.V., Patil, S., et al. (2022). Polysaccharide-drug conjugates: A tool for enhanced cancer therapy. Polymers, 14(5): 950. https://doi.org/10.3390/polym14050950
[33] Khalaji, S., Golshan Ebrahimi, N., Hosseinkhani, H. (2021). Enhancement of biocompatibility of PVA/HTCC blend polymer with collagen for skin care application. International Journal of Polymeric Materials and Polymeric Biomaterials, 70(7): 459-468. https://doi.org/10.1080/00914037.2020.1725761